Optical Measurements of Exhaust Process of an Electrothermal Pulsed Plasma Thruster†

MIYASAKA Takeshi*, KOBAYASHI Akira, and ASATO Katsuo***

Abstract

Pulsed Plasma Thrusters (PPT) are electrothermal and electromagnetic thrusters to produce thrust in a discharge. A coaxial PPT with solid propellant has been designed and operated in Gifu University. To examine unsteady characteristics in the discharge process of the PPT, measurements using a high speed camera and a triple Langmuir probe were carried out. The time variances of luminescence from the PPT were observed for various cavity geometries. As a result, a strong correlation was observed between the intensity of the luminescence and the cavity geometry. Measurements of the PPT using photosensors for the luminescence behavior caused by plasma generation and exhaust were carried out. Plume measurements for different cavity geometries were performed using a photosensor system incorporating optical fibers, which was developed in this study. As a result, it was found that difference in the time lag of the exhaust plasma behind the discharge current peak for all cavity geometries depended on the distance from the nozzle.

KEY WORDS: (Electric propulsion), (Pulsed plasma thruster), (Solid propellant), (Luminescence), (High speed camera), (Coaxial)

1. Introduction

The pulsed plasma thruster (PPT) with solid propellant is promising as a space propulsion system from a viewpoint of compactness and lightweight[1]. Because the PPT can be operated at low power and generate low thrust as a pulse, it is promising as an accurate posture control device for micro satellites or precise attitude control devices of large flexible structures. Experimental and numerical studies on the PPT have been performed by numerous workers [1-19]. Development and researches of coaxial PPTs have also been carried out in Gifu University[1-15] .

In the present study, to examine fundamental characteristics of the PPT, preliminary measurements were performed. Discharge current profiles for various capacitor energy and cavity geometries were measured using a Rogovsky coil. Using a high-speed camera, luminescence images from PPT were taken. Electric number density and temperature of plume were measured using a triple Langmuir probe. By comparing the photographs with the results of the discharge current profiles and the plume characteristics for various cavity geometries, unsteady discharge phenomena of the PPT were investigated. Equivalent plasma resistance was also evaluated by LCR analysis. The results of the LCR analyses were used to investigate a relation between the amount of ablation and the cavity geometries.

Quantitative measurements of luminescence from a PPT have been carried out by Takegahara et al. using a photo-diode[19]. However, in our experimental environment, the same measurement was difficult because there was considerable electromagnetic noise in the luminescence profiles. Thus, in the present study, a photosensor system consisting of an APD (avalanche photodiode) module and optical fibers was developed and the luminescence from a PPT named "GOS-II" was measured. The photosensor system enabled measurements with less noise and high sensitivity. In the present paper, we describe the results of multipoint measurements of luminescence from the plume for various cavity geometries, using the developed photosensor system, and discuss the influence of the cavity geometry on the luminescence profiles and the relationship of the results with the discharge current profiles.

2. Operation of Electrothermal PPT

A schematic of the experimental setup of the PPT measurements of the present study is shown in **Fig.1**. The divergent nozzle is also used as a cathode and an anode column is set inside a Teflon® tube. The electrodes are made of stainless steel. The photographs of the PPT is

† Received on June 18, 2012
* Gifu University
** JWRI, Osaka University
Transactions of JWRI is published by Joining and Welding Research Institute, Osaka University, Ibaraki, Osaka 567-0047, Japan

shown in **Fig.2**. **Figure 3** shows the operation of the PPT. For the purpose of preliminary and direct optical measurements, the PPT is mounted inside the small glass chamber. Therefore, the capacitor is installed out of the vacuum chamber. The igniter is set up in the cathode nozzle at a distance 3mm apart from the Teflon® tube end. The time variance of a discharge current was measured by the Rogovsky coil. The current profiles were used for LCR analyses using the assumption of constant resistance and inductance[1, 3]:

$$I(t) = A\exp(-Bt)\sin\omega t \qquad \text{-------- (1)}$$

Thus, the equivalent total resistance $R_{total,eq}$ is obtained from the following equations:

$$B = \frac{2}{T}\ln(I_1/I_2) \qquad \text{-------- (2)}$$

$$R_{total,eq} = \frac{2B/C}{\omega^2 + B^2} \qquad \text{-------- (3)}$$

where C, I_1, and I_2 are the capacitance, the first and second peak values of the discharge current, respectively and the period T is determined from a time interval between the peaks (see **Fig. 4**).

The capacitance of the capacitor used for the present study is 4 μF.

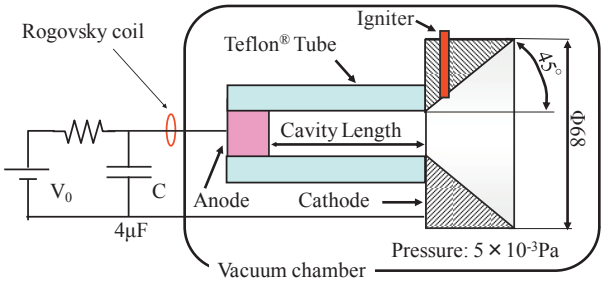

Fig. 1 Schematic of experimental setup.

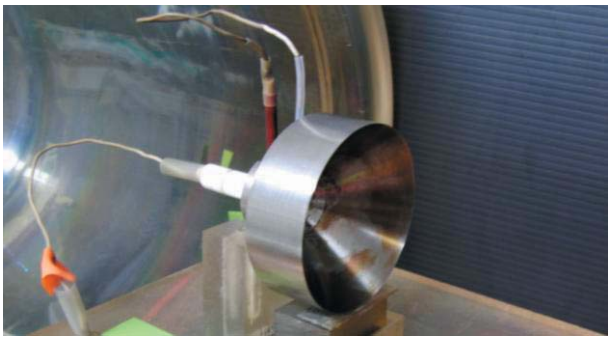

Fig. 2 Photograph of Gifu University PPT named "GOS-II".

3. Investigations of Fundamental Characteristics

First, to clarify fundamental characteristics of the Gifu Univ. PPT, preliminary investigations were carried out for various capacitor energies and cavity geometries by triple probe measurements, high speed camera photography, and LCR analyses. Various cavities having a diameter of 2mm and 3mm and a length of 5 to 25 mm were used for the present experiments. The capacitor energy was set at 4 to 16 J.

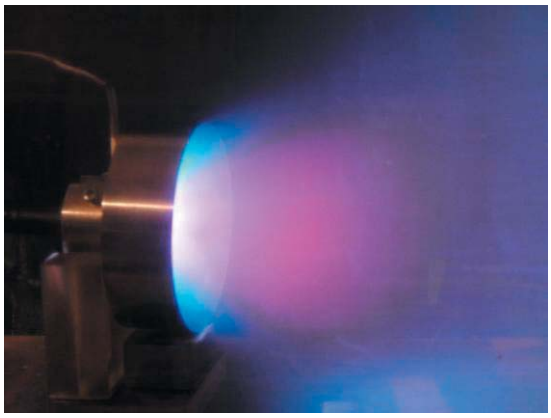

Fig. 3 Photograph of operation of GOS-II.

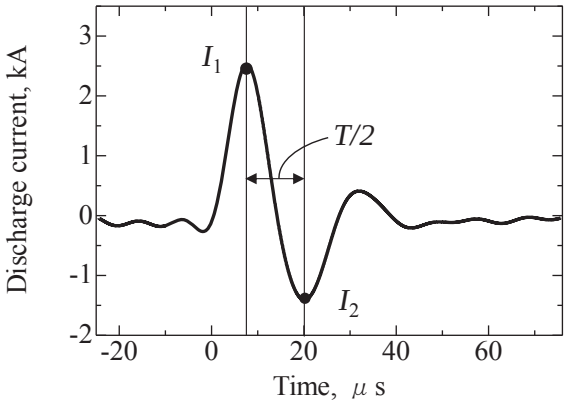

Fig. 4 Example of discharge current profile.

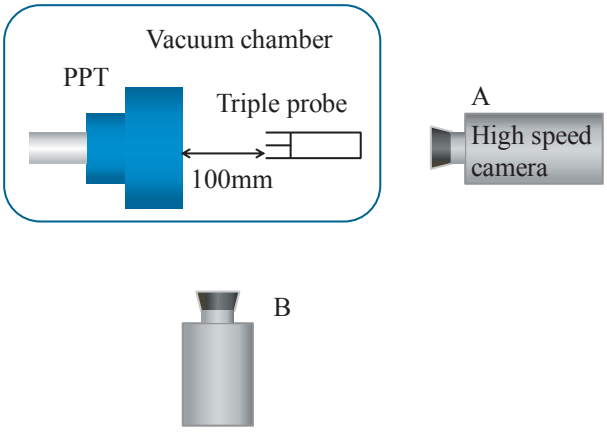

Fig. 5 Measurement setup of high-speed camera and triple probe.

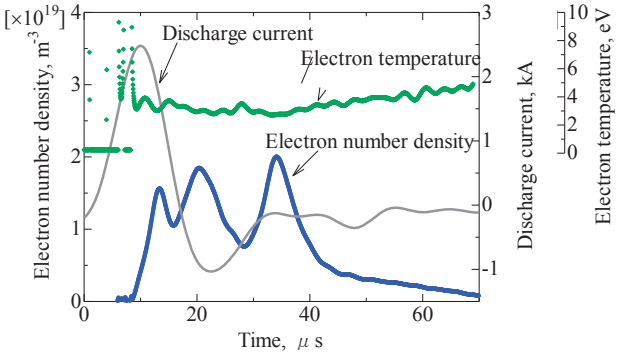

Fig. 6 Example profiles of discharge current, electron temperature, and electron number density.

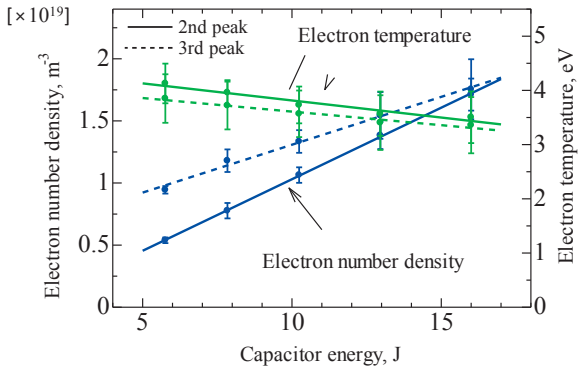

Fig. 7 Dependencies of electron temperature and electron number density on capacitor energy.

3.1 High speed photography

Photographs of luminescence patterns from the PPT were taken using a high speed camera, NAC FS501 (see **Fig. 5**). It can take photographs at 2,000-20,000,000 fps with an exposure time of 10 ns-20 μs, an interframe distance of 40 ns-320 μs, and the time resolution of 0.5-50 ns. In the present study, a pulse signal of the igniter was used as the trigger for the high speed camera. Successive 18 photographs from the downstream of the nozzle were taken at exposure of 100ns and frame intervals of 2.9 μs. The photographs from the horizontal direction were also taken at exposure of 1 μs and frame intervals of 2 μs.

3.2 A triple Langmuir probe measurement

A triple Langmuir probe was used to obtain the time variance of electron temperature and number density of plasma plume. The two probe currents are measured by current probes, Tektronix TCP312 with the voltages of 10 and 30 V.

3.3 Results and Discussion

3.3.1 Plume characteristics

The electron temperature and the electron number density for various capacitor energies were measured by a triple Langmuir probe at 100 mm downstream of the exit plane. The fixed cavity geometries, diameter of 3 mm and length of 25 mm were used. **Figure 6** shows the results for a capacitor energy of 16 J. As in Fig.5, the electron number density has three peaks. The second and third peak values for various capacitor energies are plotted in **Fig. 7**. The electron temperature at the peak time is also shown in Fig. 7. In each case, an increase of the value of the electron number density is observed for larger capacitor energy. This indicates the increase in the amount of ablated gas from the propellant surface with increasing energy. The strong increase of the ablation causes the decrease in the energy per mass of the ablated gas. Consequently, the temperature of each peak decreases as the energy increases as shown in Fig. 6.

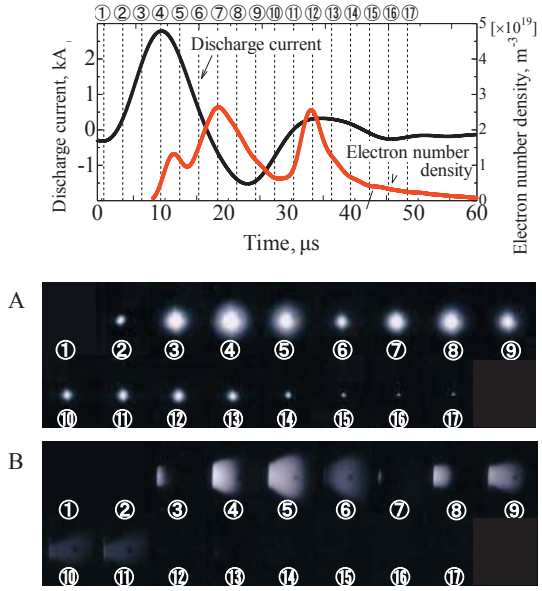

Fig. 8 Profiles of discharge current and electron number density and successive photographs from two directions for cavity length of 15 mm.

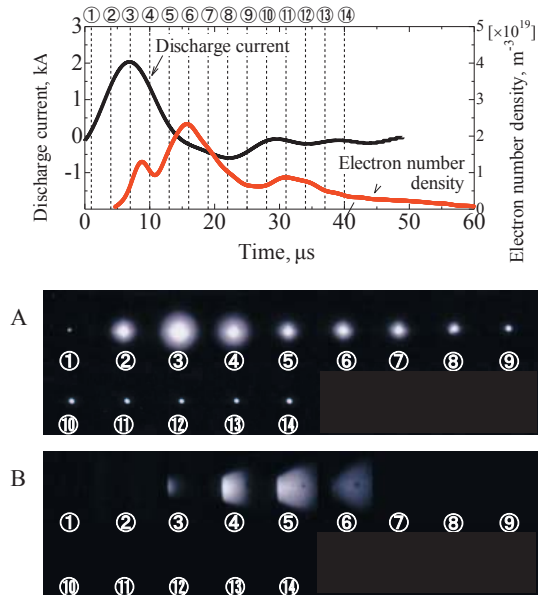

Fig. 9 Profiles of discharge current and electron number density and successive photographs from two directions for cavity length of 25 mm.

3.3.2 Unsteady discharge and luminescence from the PPT

Figure 8 shows successive photographs taken from the downstream (A) and horizontal direction (B) (see Fig.4) for a cavity diameter of 2 mm and length of 15 mm. The photographs are shown with profiles of the discharge current and the electron number density. The results for a diameter of 2 mm and length of 25 mm are also shown in **Fig. 9**. The capacitor energy for each case is 16 J. The electron number density was measured at 100 mm downstream of the exit plane using a triple Langmuir probe.

In Figs. 8 and 9, each peak of luminescence intensity from the downstream is observed 1 or 2 flames after the peak from downstream. This indicates that the photographs show the luminescence from the plasma which is generated and exhausted.

The discharge current for each cavity length has two clear peaks. However, the second peak of the current for cavity length of 25 mm is weaker compared with the other peaks. Similar behavior was recognized in the electron number density profiles. These tendencies are consistent with that of the luminescence intensity. These results indicate that the second and third peaks of the electron number density are those of plasma generated by the main discharge.

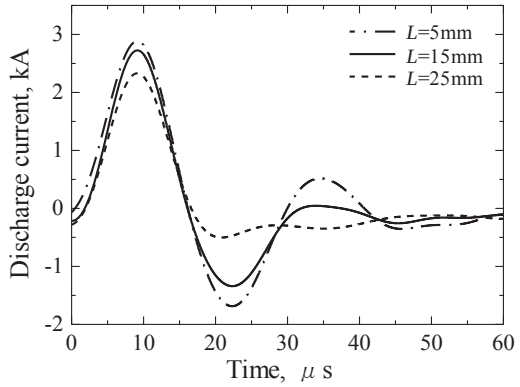

Fig. 10 Dependence of discharge current profile on cavity length for cavity diameter of 2 mm.

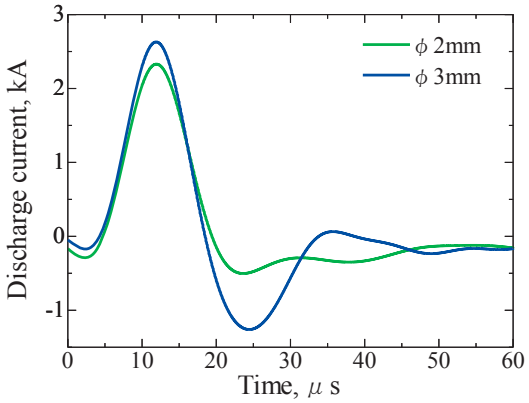

Fig. 11 Dependence of discharge current profile on cavity diameter for cavity length of 25 mm.

3.3.3 Equivalent plasma resistance and transfer efficiency

The discharge current profiles for various cavity geometries and fixed capacitor energy of 16 J are shown in **Figs. 10 and 11**. These figures show the discharge current profiles for diameter of 2 mm and various lengths and for length of 25 mm and two different diameters, respectively. The discharge currents draw typical profiles of dumped oscillation. The amplitude decreased with increasing the cavity length due to the increase of the plasma resistance between the electrodes.

To estimate the plasma resistance, LCR analyses were carried out. **Figure 12** shows the total equivalent resistance $R_{total,eq}$ and the equivalent plasma resistance $R_{p,eq}$ for various cavity geometries. $R_{p,eq}$ was obtained from $R_{total,eq}$ and the resistance of the LCR circuit except the plasma $R_{cir,eq}$ by the following relation:

$$R_{p,eq} = R_{total,eq} - R_{cir,eq} \qquad \text{-------- (4)}$$

$R_{total,eq}$ is calculated by the LCR analysis using the discharge current profile. By averaging two values of $R_{total,eq}(L=0)$ estimated using the values for shorter cavity lengths, $R_{cir,eq}$ was estimated. The equivalent plasma resistance increases for longer cavity length or smaller

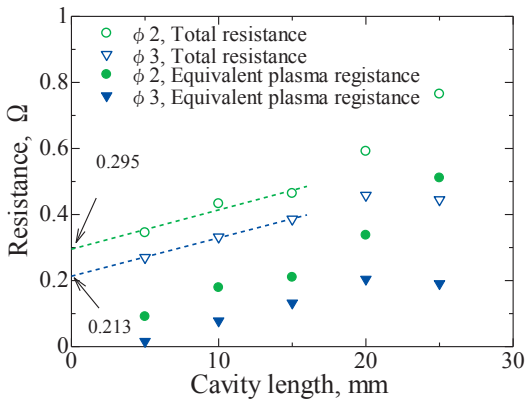

Fig. 12 Equivalence resistance versus cavity length.

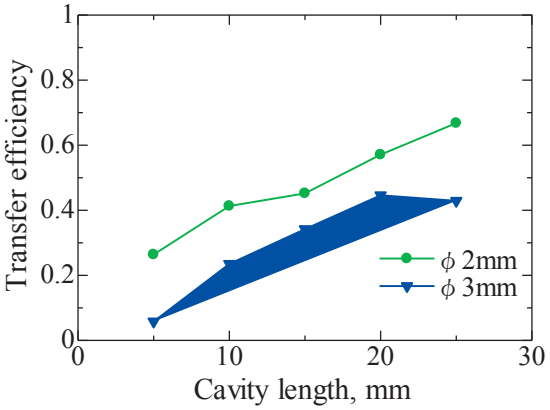

Fig. 13 Transfer efficiency versus cavity length.

diameter, as seen in the past works. The tendency is approximately similar to the results of the discharge diameter, as seen in the past works. The tendency is current amplitude. In the case of a cavity diameter of 3 mm, the increase in the resistance is not observed for longer cavity length of more than 20 mm. This indicates that only from the view point of plasma generation, the cavity length of 20 mm is the most suitable condition for a diameter of 3 mm. Also for diameter of 2 mm, the peak of the resistance must appear for a cavity length of more than 25 mm. The estimated transfer efficiency using the resistances is shown in **Fig. 13**. The efficiency will be improved by reducing the circuit resistance[2].

4. Luminescence Measurements of Unsteady Characteristics of Plume

To find optimum design and operational conditions, investigations of unsteady characteristics of the PPT plume are required. However, in methods using electrical cables, electromagnetic noise strongly affects the luminescence profiles. Thus, in this study, to enable noncontact and quantitative measurements of the unsteady PPT plume, a high-sensitivity photosensor system with optical fibers was developed. We carried out the measurements of luminescence from the plume of the PPT for various cavity geometries and the fundamental validation of the photosensor system. We also investigated the influence of the cavity geometry on the peak time of measured luminescence profiles. In the measurements, the fixed capacitor energy of 8 J was used for the present measurements.

4.1 Photosensor system with optical fibers

Instead of setting the photodiode inside the glass chamber and using a current cable connected to an oscilloscope, we use optical fibers and keep the photodiode away from the PPT system to remove the influence of electromagnetic noise arising from PPT operation with a high discharge current on the profiles detected with the photodiode.

However, the use of an optical fiber decreases the amount of light detected with the photodiode. Thus, when an optical fiber and a normal photodiode are used, the amount of light is insufficient for analyzing the luminescence profile with high spatial resolution in unsteady PPT operation in which multiple luminescence peaks are observed. Therefore, an avalanche photodiode (APD) module, C5331-04 (Hamamatsu Photonics), was used in the present luminescence measurement. The APD module enables high-sensitivity optical detection. In addition, a temperature-compensated bias voltage circuit and high-speed current to voltage amplifier circuit of the module can keep the gain constant and enable high time resolution. The gain and the active area are 30 and 3 mm, respectively. The frequency bandwidth and spectral response range are 4 k to 80 MHz and 400 to 1000 nm, respectively.

A schematic of the photosensor system developed in this study is shown in **Fig. 14**. As shown, three optical fibers were mounted 10, 30, and 50 mm downstream of the cathode nozzle. The active area of the fiber is 1 mm. Each luminescence from the plume was transported through the optical fibers and was detected by the respective APD module. In addition, the APD module was mounted well away from the chamber. Therefore, no significant electromagnetic noise was observed.

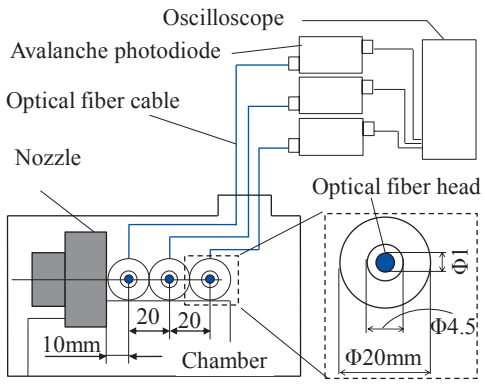

Fig. 14 Measurement setup of photosensor system using optical fiber cables.

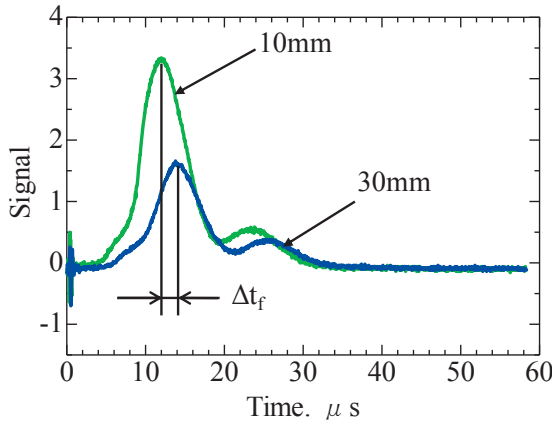

(a) Collimator diameter of 4.5 mm.

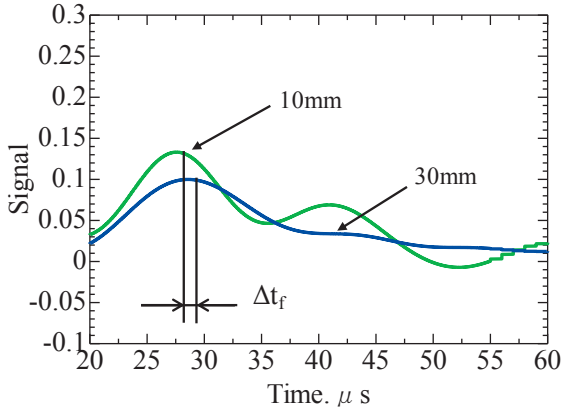

(b) Collimator diameter of 0.5 mm.

Fig. 15 Comparison between luminescence profiles at 10 and 30 mm downstream of nozzle end for collimator diameters of 4.5 and 0.5 mm.

One of the main purposes of the multipoint measurement of the luminescence from the plume is to estimate the plume velocity using the luminescence peaks by a time-of-flight method. Thus, space resolution is important in this measurement. A collimator is mounted in front of the fiber head. However, strong localization by the collimator causes a decrease in the intensity of the signal of the detected luminescence, and time resolution becomes poor. Therefore, first, measurements for different collimators were carried out. **Figure 15** shows the comparison between luminescence profiles for the collimator diameters of 4.5 and 0.5 mm. The distance between the collimator and fiber head is 10 mm in each case. The profiles for two collimators show multiple peaks. Although the profiles observed 10 and 30 mm downstream of the cathode nozzle end for the larger collimator diameter of 4.5 mm show three clear peaks, the peaks for the smaller diameter of 0.5 mm are unclear, and the third peak of the profile observed 30 mm downstream of the end is indistinct. In addition, the time difference between the peak times observed at two measurement points are almost the same for the two collimators. This suggests that the collimator with the diameter of 4.5 mm gives sufficient spatial resolution for the estimation by the time-of-flight method. For these reasons, the collimator with the diameter of 4.5 mm was employed in this study.

4.2 Multipoint measurement of luminescence from plume using photosensor system

The measurements of the luminescence from the plume were carried out for various cavity geometries. In this study, propellants with different cylindrical cavity geometries, were used. By varying the length and diameter of the cavity, we investigated the influence of the cavity geometry on the operation of the PPT.

First, the profiles of luminescence measured at three axial positions, 10, 30, and 50 mm downstream of the cathode nozzle end are shown in **Fig. 16**. The length and diameter are 25 and 3 mm respectively. In each profile, two clear peaks with nominal electromagnetic noise are confirmed. These peaks appear later as the distance and diameter of the cavity used for the measurement from the nozzle end increases. These results confirm the effectiveness of the capturing process of exhaust from the cathode nozzle. Accordingly, comparison of these peak times allows the clarification of the exhaust characteristics of the plume. Unlike analyses using high-speed photography, the present method of using the photosensor system can allow quantitative comparisons. However, the profile measured 50 mm downstream of the nozzle end still shows smaller peaks compared with those at the other measurement points, and makes comparison with high resolution difficult. Therefore, the following investigations were carried out using the results measured at two closer points, 10 and 30 mm.

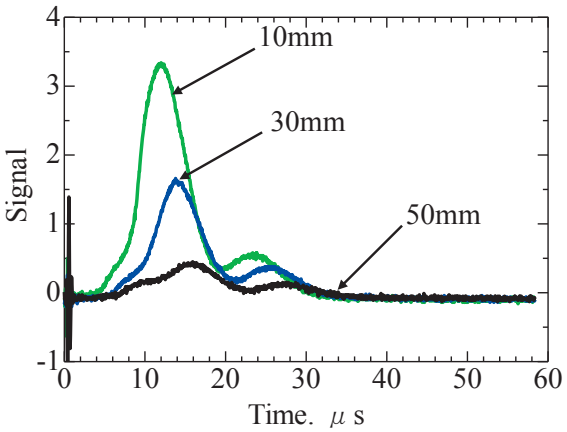

Fig. 16 Profiles of luminescence measured at three axial positions, 10, 30, and 50 mm downstream of nozzle end.

4.3 High speed photography

To confirm the photosensor system measurements, plume velocities were also estimated by simultaneous photography of luminescence from the propellant part and the plume using a high-speed camera. The high-speed camera, NAC - FS501, was also used for the photography. Simultaneous photography was confirmed for various propellant cavity geometries (see **Fig. 17**) . An example of the photograph is given in **Fig. 18**.

4.4 Results and discussion

Figure 19 shows the profiles of luminescence measured at two measurement points using the photo-

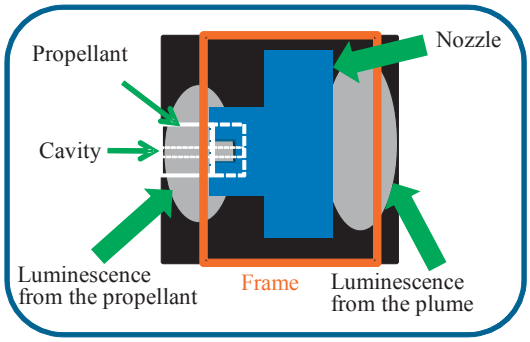

Fig. 17 Schematic of simultaneous photography of luminescence from propellant part and plume by high-speed camera.

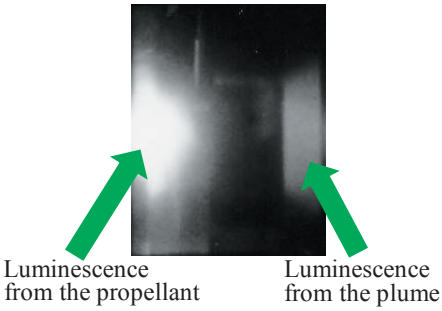

Fig. 18 Example photograph of simultaneous photography of luminescence from propellant part and plume by high-speed camera.

sensor system and the discharge current profile for three different cavity geometries. These three different cavity geometries are described in **Table 1**. In addition, the photographs of plume peak luminescence obtained by high-speed photography, which corresponds to the peak of the profile measured using the photosensor system, are also shown in Fig. 19. In cases (a) and (b), the discharge current profiles show two clear peaks, and the corresponding peaks are confirmed in the profiles of luminescence measured at two measurement points using the photo sensor system. In case (c), the discharge current profile has three peaks, and also, in the profiles of luminescence obtained using the photosensor system, the corresponding three peaks are observed. In addition, the relationship among the luminescence intensities of the peaks in each case corresponds to that of discharge current peaks, and also agrees well with that obtained from high speed photographs. Although in the previous study only using the photographs, detailed comparisons of the intensities of luminescence were difficult, the photosensor system makes such comparisons possible. Thus, using the luminescence profiles obtained with the photosensor system, we performed detailed time evaluations. The time-of-flight of the plume between the two measurement points Δt_f are calculated with high resolution using the time difference between the two peaks of the luminescence profile.

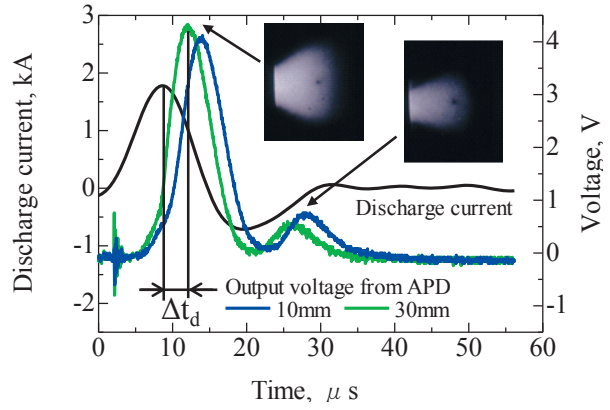

(a) Cavity length of 15 mm and diameter of 2 mm.

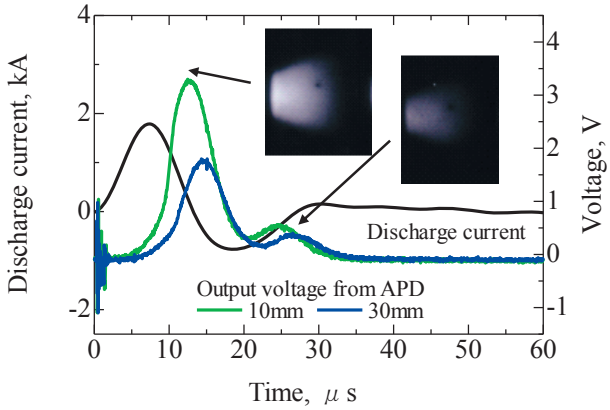

(b) Cavity length of 25 mm and diameter of 3 mm.

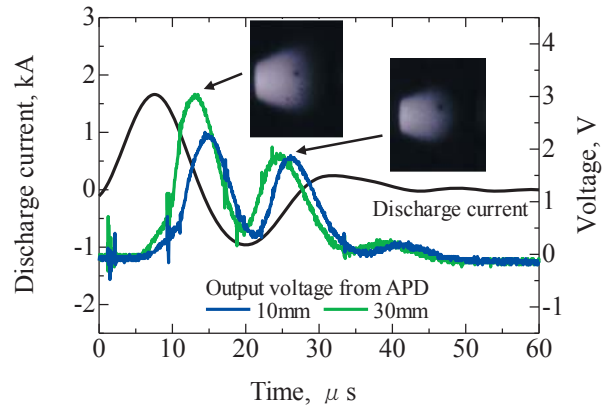

(c) Cavity length of 15 mm and diameter of 3 mm.

Fig. 19 Profiles of luminescence measured 10 and 30 mm downstream of the cathode nozzle end, discharge current profiles, and plume photographs of first and second peaks for three cavity geometries.

The plume velocities of the first and second peaks, which are obtained by the time-of-flight method, are shown in **Fig. 20**. In Fig. 20, the plume velocities estimated from the high-speed photographs are also shown. These velocities shown in Fig. 20 are normalized using the velocity obtained by the photography for case (a). Since high-speed photography is a two-dimensional measurement, the time resolution is low. Thus, the velocities for each case show the same value. In the result obtained using the photosensor system, the plume velocities of the first and second peaks for three cavity geometries are within 16 % and the average velocity in each case agrees well with that obtained from the high speed photographs.

Figure 21 shows the time lags of the first peak of luminescence behind that of the discharge current Δt_d for the three cavity geometries. The time lags of the shooting time of the first brightest image of the successive high-

Table 1 Three different cavity geometries used for luminescence measurements.

	Case (a)	Case (b)	Case (c)
Diameter	2 mm	3 mm	3 mm
Length	15 mm	25 mm	15 mm

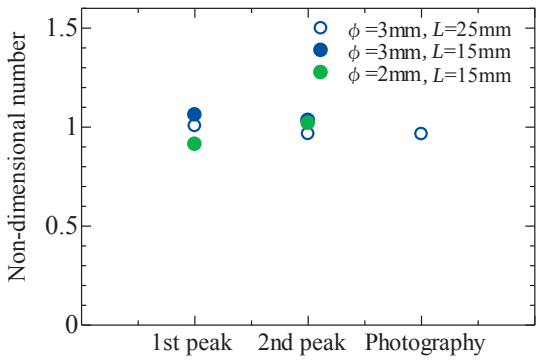

Fig. 20 Non-dimensionalized plume velocities of plume of first and second peaks estimated from photosensor results for three cavity geometries and results of first peak obtained by high-speed photography.

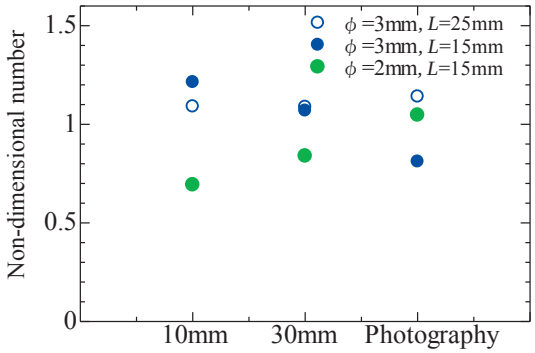

Fig. 21 Non-dimensionalized time lags of first peak of plume luminescence behind that of discharge current for three cavity geometries and results obtained by high-speed photography.

speed photographs of the plume are also shown in Fig. 21. These velocities shown in Fig. 21 are also normalized using the velocity obtained by the photography for case (a). Figure 21 indicates that the influence of the cavity geometry on the time lag depends on the distance from the cathode nozzle end. As the distance of the measurement point increases, the result appears similar to the result of high-speed photography.

5. Conclusions

First, to clarify characteristics of the Gifu Univ. PPT, preliminary investigations were carried out for various capacitor energies and cavity geometries by triple probe measurements and high speed camera photography. In the triple probe measurements, the increase of the electron number density and the decrease of the electron temperature with increasing the capacitor energy were observed. The successive luminescence images from the PPT by the high speed camera photography suggest that there is a strong correlation between the time variance of the amount of the exhaust plasma and the discharge current profile. In addition, the equivalent plasma resistances for various cavity geometries were estimated from the currents profiles measured using a Rogovski coil by LCR analyses. The LCR analyses reveal that the equivalent plasma resistance increases for smaller or longer cavity and has a peak for cavity diameter of 3mm.

To investigate unsteady characteristics of the electrothermal PPT for the derivations of optimum design and operational conditions of the electrothermal PPT, a high sensitivity-photosensor system with optical fibers was developed. Using the developed photosensor system clear profiles of luminescence from the plume with little electromagnetic noise were obtained. The results show the fundamental validation of the photosensor system for luminescence measurements of the PPT. The luminescence measurements of the plume were carried out for various cavity geometries. The velocities estimated from the time difference between the first and second peaks correspond approximately to those obtained using the photographs. The influence of the cavity geometry on the time lag of the profile peak obtained with the photosensor system behind that of the discharge current profile depends on the axial distance of the measurement from the cathode nozzle end. The influence moves closer to the result of high-speed photography as the measurement distance increases.

Acknowledgement

Authors would like to thank members of the PPT research Group in Gifu University for their assistantces, Professor Yoshihiro Arakawa for his support of vacuum system and also Professor Haruki Takegahara, Professor Hirokazu Tahara, Professor Masakatsu Nakano, and Dr. Satoshi Kakami for their helpful discussions.

References

1) K. Kuriki and Y. Arakawa, Introduction to Electric Propulsion (in Japanese), Univ. of Tokyo Press, 2003.
2) T. Edamitsu, Doctor Thesis (in Japanese) (2006), Osaka Univ.
3) A. Kakami, Doctor Thesis (in Japanese) (2002), Univ. of Tokyo.
4) M. Mukai, Y. Kamishima, T. Sasaki, K. Shintani, J. Aoyagi, and H. Takegahara, Proc. of the 30th International Electric Propulsion Conference, IEPC-2007-243 (2007).
5) T. Saito, H. Koizumi, and H. Kuninaka, Proc. of the 30th International Electric Propulsion Conference, IEPC-2007-116(2007).
6) A. K. Hallock, E. Choueiri, and K. A. Polzon, Proc. of the 30th International Electric Propulsion Conference, IEPC-2007-165, 2007.
7) A. Kakami, K. Koizumi, K. Komurasaki, and Y. Arakawa, Design and Performance of a Pulsed Plasma Thruster with Liquid Propellants, Advances in Applied Plasma Science, **4** (2003), pp.127-132.
8) T. Edamitsu, H. Tahara, and T. Yoshikawa, Proc. of Asian Joint Conference on Propulsion and Power 2005, AJCPP2005-22083(2005).
9) H. Koizumi, R. Noji, K. Komurasaki, and Y. Arakawa, Proc. of the 30th International Electric Propulsion Conference, IEPC-2007-189(2007).
10) E. J. Beiting, J. Qian, R. W. Russell, and J. E. Pollard, W. Caven, and R. Corey, Proc. of the 30th International Electric Propulsion Conference, IEPC-2007-268(2007).
11) H. Okabe, T. Miyasaka, K. Asato, and S. Sato, Frontier of Applied Plasma Technology, **1** (2008), pp.33-36.
12) T. Miyasaka, K. Asato, S. Sato and H. Okabe, Applied Plasma Science, **16** (2008), pp.113-118. (in Japanese)
13) T. Miyasaka, S. Sato, and K. Asato, Transactions of the Japan Society for Aeronautical and Space Sciences, Aerospace Technology Japan, **8** (2010) Pb_103-Pb_108.
14) T. Miyasaka S. Sato, K. Asato, Frontier of Applied Plasma Technology, **3** (2010), pp.79-84.
15) T. Miyasaka, K. Asato, N. Sakaguchi, and K. Ito, Vacuum, in press.
16) T. E. Markusic and R. A. Spores, AIAA 97-2924(1997).
17) G. A. Popov and N. N. Antropov, Acta Astronautica, **59** (2006), pp.175-180.
18) M. Keidar, I. D. Boyd, and I. I. Beilis, J. of Propulsion and Power, **19** (2003), pp.424-430.
19) H. Matsui, Y. Kubota, T. Sasaki, M. Mukai, G. Shintani, J. Aoyagi, and H. Takegahara, Proc. of Sapce Transportation Symposium (2008), pp.475-478 (in Japanese).